

# Application of cohesive crack model to simulation of rocks mechanical behavior in grain-based distinct element model

Hadi Fathipour-Azar<sup>a,\*</sup>, Seyed-Mohammad Esmail Jalali<sup>a</sup>, Seyed Rahman Torabi<sup>a</sup>

<sup>a</sup> Department of Mining Eng, Petroleum and Geophysics, Shahrood University of Technology, Shahrood, Iran

## Article History:

Received: 03 November 2018,

Revised: 10 June 2019

Accepted: 28 August 2019.

## ABSTRACT

This paper aims to study the mechanical behavior of rocks subjected to different mechanical loading conditions using the Cohesive Crack Model (CCM) and Grain-Based Model (GBM) in the Distinct Element Method (DEM) simulations. In the GBM-DEM, the Voronoi tessellation scheme is used, and intact materials are simulated as a collection of structural units (particles/blocks) bonded together at their contact areas. Implementing the CCM revealed a nonlinear behavior of grain interfaces under various loading modes. Numerical simulation of a tension-compression and direct shear test was conducted to verify that the CCM was implemented correctly. The simulated numerical curves were consistent to the results of theoretical calculations, indicating that the model incorporated into GBM-DEM could simulate more realistically similar to the micro-cracking mechanisms. Finally, CCM was used to simulate the uniaxial and biaxial compression tests under the Universal Distinct Element Code (UDEC). The results of the models were in a good agreement with the relevant responses of the rock under different loading conditions, verifying the applicability of the CCM.

**Keywords :** Cohesive crack model; Grain-based distinct element model; Interface; Constitutive model; Calibration

## 1. Introduction

The mechanical behavior of rock is strongly affected by its micro properties, such as grains and contact parameters of cohesive interfaces [1-3]. The evaluation of the mechanical behavior of rock is still of great importance in geomechanics and civil engineering. In recent years, a considerable number of grain-based numerical investigations has been performed based on the discrete element method (DEM) simulations to reproduce many mechanical features of rocks in a laboratory and large-scale experiments. This approach has been used to study progressive damage in slow-moving landslides [4] within the disturbance zone around underground openings [5], typical rock slope failure mechanisms [6], effects of grain-scale heterogeneities [7,8], intra-granular failure [9], mesh geometry dependencies [10], scale dependency of rock mass properties [11], estimating the confined strength of rock blocks considering scale effects and in-situ heterogeneity [12].

In DEM modeling, the interaction between inter particles/blocks is explicitly considered to simulate the mechanical behavior and fracture of rocks [13]. The two most known commercial DEM codes are Universal Distinct Element Code (UDEC) and Particle Flow Code (PFC). In PFC, the intact material is simulated as a collection of rounded particles while in UDEC Voronoi models, and using the Voronoi tessellation generator, the specified domain is represented by densely packed rigids, deformable polygons, or trigon particles, which are bonded together and interact one another at their contact points [14]. Voronoi models are often mentioned as Damage Models (DM) or Grain-Based/Boundary Models (GBM) or Particle/Block Bonded Models (PBM). Micro fracturing, i.e., initiation and propagation of cracks along grain boundaries of rocks, and are controlled by predefined contact micro properties and the interaction contact constitutive law.

Therefore, damage, in the form of broken bonds, can be captured [8,15], which can coalesce into a macroscopic fracture.

Although PFC is widely used in geomechanical engineering problems to reproduce many mechanical features of rocks, it suffers from an underestimation of tensile strength, for instance. The underestimation of tensile strength in PFC could be because rounded particles cannot appropriately represent the irregular-shaped and interlocked grains of rock. In order to solve this drawback, different solutions, such as clustering [16], clumping [17], logic and grain-based models (GBM) [18], and flat-joint models [19] are used. However, despite many efforts, challenges still remain [20]. Moreover, a more desirable and explicit representation of rock texture is polygonal, rather than circular, representation of grains [3].

In the GBM-UDEC, micromechanical parameters cannot be easily measured in the laboratory or directly related to either measurable or physical material parameters. Therefore, a calibration process is required, in which the micro properties are chosen to match laboratory tests or field results of the rock material. In the trial and error calibration process, several procedures were suggested to reproduce the model response by performing uniaxial, triaxial, and Brazilian tests [1, 14,21]. Generally, a variation of contact stiffness and the stiffness ratio affected the Elastic modulus and Poisson's ratio. While shear strength properties led to variants in uniaxial and biaxial compressive strengths.

Modeling displacement stress relationships of the interfaces/contacts are essential for realistic numerical simulation and failure analysis of geomaterial. In numerical analysis of an intact rock, a generally linear contact model is used. In this approach, the behavior of intact material is assumed to be a linear and nonlinear zone in front of a crack tip in damage stage, known as fracture process zone (FPZ), which is also considered to be negligible [22]. However, it has long been recognized that in quasi-brittle materials, such as rocks, concrete, and soil, this state is not always true. Also, such behaviors have been proven to be

\* Corresponding author. Tel.: +98-9143262051. E-mail address: fathipour.hadi@gmail.com (H. Fathipour-Azar).

representative of hard rocks [23]. The nonlinearity in FPZ is characterized by the Cohesive Crack Model (CCM), as illustrated in Fig. 1. Based on the user-defined failure criterion, CCM allows the initiation of new fractures and facilitates the use of physical concepts, such as critical energy release rate, for simulating the growth and opening/sliding of fractures [1,11,21,24].

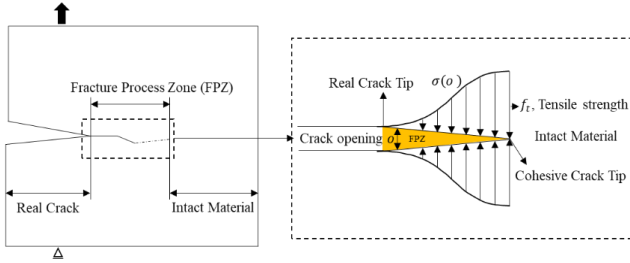


Fig. 1. Characterization of the cohesive crack model.

The objective of this study is to implement CCM as a constitutive law for the behavior of particle boundaries in GBM-UDEC to represent more realistic models of the progressive degradation and failure mechanism of geomaterials under various loading regimes applied to geomechanical problems. In order to achieve this objective, the compressive-tension and shear test was performed for model validation, and then conventional laboratory tests such as uniaxial, biaxial compressive tests were performed numerically using the implemented CCM in UDEC GBM. In order to show the performance of the proposed model, the results were compared with typical and obtained laboratory values.

## 2. Interface constitutive law of cohesive crack model for inter-granular cracking

Mechanism-based concepts provide key insights into supporting the development of computational models to predict crack initiation and propagation in the material. The Cohesive Crack Models (CCM) were introduced by Dugdale [25], Barenblatt [26], and later extended by

Hillerborg et al. [27], in which the constitute interaction law governs the mechanical load exchanging across the contact boundaries. In this study, CCM [11], with the unloading-loading feature, was adopted to characterize the nonlinear relationship between relative displacements and the stress inside the FPZ. Therefore, this method appropriately reflects the mechanical behaviors and failure characteristics of the grain interfaces (as shown in Fig. 1). In the FPZ, for a 2D case, stress exists in normal and shear directions across the crack surface, and the corresponding relative displacements are  $o$  and  $s$ . Fig. 2 shows a typical nonlinear stress displacement response for the Tensile Cracking Mode (Mode I) and the Shear Cracking Mode (Mode II). In Mode I, the contact interface follows a nonlinear elastic constitutive behavior at the tip of the crack opening (as shown in Fig. 2a). This behavior shows the decay of stiffness in the pre-failure state owing to the progression of damage. The interface starts to yield when the crack opening ( $o$ ) reaches the critical value of  $o_p$ , which can be calculated by the following equation:

$$o_p = e \frac{f_t}{k_t} \quad (1)$$

where,  $e = \exp(1)$  is the base of the natural logarithm,  $f_t$  is the intrinsic tensile strength of the rock material obtained from laboratory experiments, and  $k_t$  is the contact initial normal stiffness value. Next, a nonlinear softening behavior is captured until the residual opening value ( $o_{res}$ ) is reached, and the contact interface finally breaks. In the softening stage of Mode I and Mode II of fracturing, the decay in the bonding stress is defined by softening function proposed by Evans and Marathe [28] based on experimental results as:

$$\chi(D_i) = \left[ 1 - \frac{a+b-1}{a+b} e^{D_i(a+cb)/((a+b)(1-a-b))} \right] \times [a(1-D_i) + b(1-D_i)^c] \quad (2)$$

where  $a$ ,  $b$ , and  $c$  are empirical curve fitting parameters equal to 0.63, 1.8, and 6.0, respectively; and  $D_i$  ( $i = I, II, I-II$ ) is a damage variable with a value between 0 and 1.  $D_i$  for ( $o_p < o < o_{res}$ ) defined as:

$$D_i = \frac{o - o_p}{o_{res} - o_p} \quad (3)$$

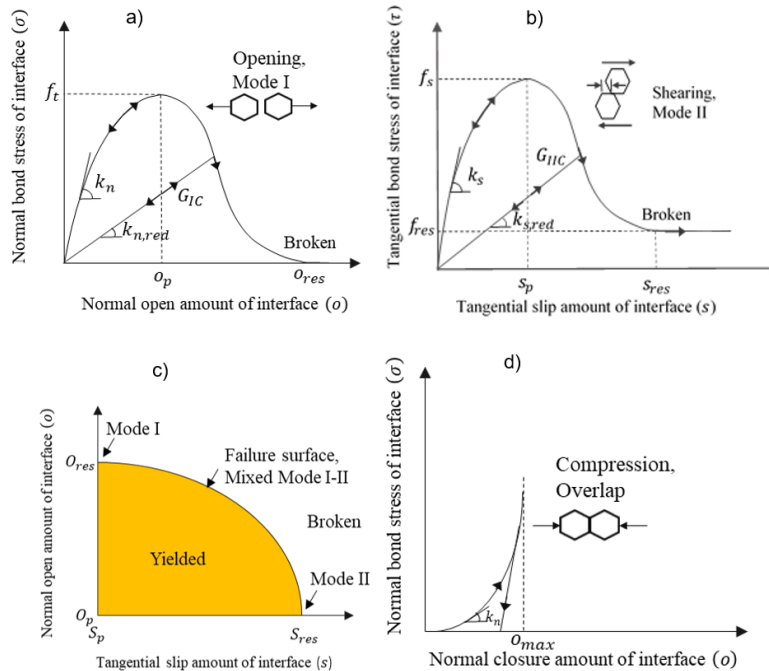


Fig. 2. Constitutive relations of cohesive contact interface elements. A) Under tension, b) shear, c) Mixed Mode, d) compression conditions.

The residual opening value  $o_{res}$  can be determined by  $o_{res} = o_p + \frac{3G_{IC}}{f_t}$ .  $G_{IC}$  is fracture energy of Mode I ( $G_{IC} = \frac{K_{IC}^2}{E}$ ), the area under the curve in Fig 2a is required to extend the crack surface of a unit area.

Therefore,  $o_{res}$  is obtained by solving this equation  $G_{IC} = \int_{o_p}^{o_{res}} \chi(D_i) f_t do$ . For unloading/reloading cycles path when  $o < o_{max}$  contact follows a linear stress displacement path where  $k_{n,red}$  is the ratio

of stress to effective displacement at  $o_{max}$  (see Fig. 2a). The constitutive law for Mode I cracking can be expressed as follows:

$$\sigma = \begin{cases} k_n \cdot o \cdot \exp\left(-\frac{o}{o_p}\right) & o < o_p \\ \chi(D_I) \cdot f_t & o_p \leq o < o_{res}, o = o_{max} \\ k_{n,red} \cdot o & o_p < o < o_{res}, o < o_{max} \\ 0 & o \geq o_{res} \end{cases} \quad (4)$$

The damage initiation criterion that is used here is the Mohr-Coulomb criterion, with a tension cut-off (Fig. 3). For a given CCM, the maximum shear stress is characterized by the normal stress,  $\sigma_n$ , cohesion,  $c$ , and internal friction angle,  $\varphi$ . Damage is assumed to initiate when the following expression is satisfied:

$$|f_s| = c + \sigma_n \tan \varphi \quad (5)$$

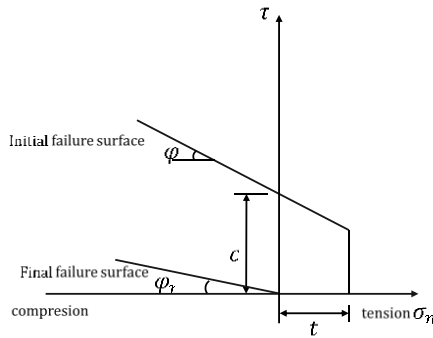


**Fig. 3.** Damage initiation criteria based on the Mohr-Coulomb model with a tension cut-off.

As shown in Fig. 2b, the contact interface behaves nonlinearly and elastically until the critical slip ( $s_p$ ). In the post-peak stage, a damage variable in the softening function can be obtained as follows:

$$D_{II} = \frac{s - s_p}{s_{res} - s_p} \quad (6)$$

As the shear slip  $s$  increases under the shear strength, the tangential stress gradually reduces to a residual friction value  $f_{res}$  once the interface experiences complete damage:

$$|f_{res}| = \sigma_n \tan \varphi_{res} \quad (7)$$

The constitutive law for Mode II cracking can be expressed as follows:

$$\sigma = \begin{cases} k_s \cdot s \cdot \exp\left(-\frac{s}{s_p}\right) & s < s_p \\ \chi(D_{II}) \cdot f_s & s_p \leq s < s_{res}, s = s_{max} \\ k_{s,red} \cdot s & s_p < s < s_{res}, s < s_{max} \\ f_{res} & s \geq s_{res} \end{cases} \quad (8)$$

The critical sliding value  $s_p$  and the residual sliding value  $s_{res}$  (by solving  $G_{IIc} = \int_{s_p}^{s_{res}} [\chi(D_{II}) \cdot f_s - f_{res}] ds$ ) are calculated as follows:

$$s_p = e \frac{f_s}{k_s} \quad (9)$$

$$s_{res} = s_p + \frac{3G_{IIc}}{f_s} \quad (10)$$

Where,  $k_s$  is the contact initial shear stiffness value, and  $G_{IIc}$  is the Mode II fracture energy. In this study, the value of  $G_{IIc}$  is considered to be two times the value of  $G_{IC}$ .

The contact interface may be subjected to a combination of opening and sliding displacements (as shown in Fig. 2c) instead of pure Mode I or pure Mode II separation. In this case, the damage variable of a contact interface is determined by:

$$D_{I-II} = \sqrt{\left(\frac{o - o_p}{o_{res} - o_p}\right)^2 + \left(\frac{s - s_p}{s_{res} - s_p}\right)^2} \quad (11)$$

It should be noted that contact damage and breakage can only happen under tension and shearing loading conditions. Although pure compression exists in numerical simulations, due to the high normal

stiffness value, no penetration is satisfied between the adjacent particles. Nonlinear compression behavior of contact under compressive normal stress (Fig. 2d) can be modeled using the following hyperbolic function, as described in Bandis et al. [29].

$$\sigma_n = \frac{k_{no} o}{1 - (o/o_{max})} \quad (12)$$

### 3. Verification of implemented CCM in UDEC

The contact interface constitutive relation, CCM (introduced in Section 2), was incorporated into UDEC by the user-defined FISH program. In the following sections, uniaxial compression, tension (Mode I), and shear (Mode II) tests were conducted for CCM verification.

#### 3.1. Uniaxial compression and tension tests

The purpose of this test is to validate the implementation of defined stress displacement behaviors of the contacts under tensile, compressive, and then shear loadings in UDEC. Carbonatite rock from the Palabora mine was used as the material for verification. The input parameters for the model were Young's modulus, Poisson's ratio, and for CCM were the initial tensile strength, initial and residual cohesion, friction and residual friction angle, and initial normal and shear stiffness, as summarized in Table 1.

**Table 1.** Typical geomechanical properties for Carbonate rock [30].

Material property	Value
Young's modulus (GPa)	60
Poisson's ratio	0.25
Density (kg/m <sup>3</sup> )	3100
Tensile strength (MPa)	10
Fracture energy (j/m <sup>2</sup> )	150
Normal stiffness (GPa/m)*	105000
Shear stiffness (GPa/m)*	94500
Cohesion, residual cohesion (MPa)*	29, 0
Friction, residual friction (°)*	54, 5
Tension, residual tension strength (MPa)*	13, 0

\* Calibrated micro-scale properties of cohesive contacts

The numerical simulation was performed on a rectangular sample having a dimension of 125×50 mm with a horizontal cohesive contact line in the middle, as shown in Fig. 4. Fig. 4(a) and (b) are respectively showing the results of uniaxial tension and uniaxial compression tests. In the first stage and in order to simulate the behavior of the contact under tension, a constant velocity ( $v_y$ ) was applied to the top external boundary of the sample, while the bottom external boundary was fixed along both x and y directions in zero displacement conditions. During modeling, the normal stress along the interface and the relative displacement were tracked. The simulated results are shown in Fig. 5. As Fig. 5 shows, all the simulation results are in good agreement with the values directly calculated from model equations for the opening-closing displacement and the tensile-compressive stress on the crack. The tensile stress initially increases with opening until it reaches the peak stress (13 MPa) at 3.37E-07 (eq. 1). Then the softening stage starts and the tensile stress on the fracture surface decreases with opening until reaching zero when the opening is at 3.49E-05 ( $o_{res}$ ). Under unloading/reloading cycles in this range, the contact follows a linear stress displacement path with normal stiffness of  $k_{n,red}$ , which is the ratio of stress to effective displacement at an unloading point. Following the breakage of the contacts, a constant velocity ( $v_y$ ) was imposed on the top external boundary. This loading condition was conducted to validate a defined approach (eq. 4) on simulating the normal stress-displacement behavior of the contact. Finally, tensile stresses were applied to the top external boundary of the upper block again to check the stress-displacement response of the broke contact in tension. The results of this numerical test show the validity of the numerical implementation of the CCM.

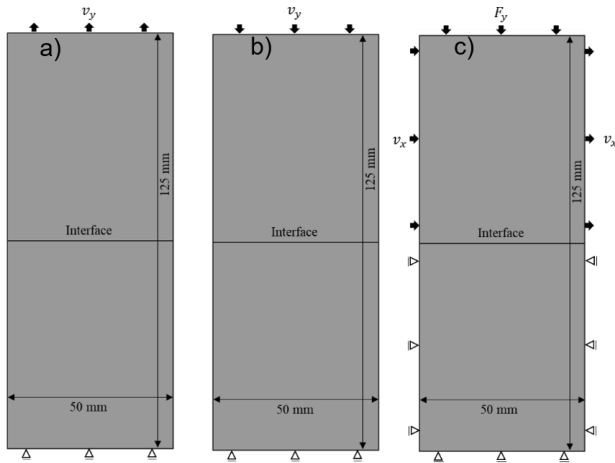


Fig. 4. The numerical models and the boundary condition in a) uniaxial tension, b) compression, c) shear tests.

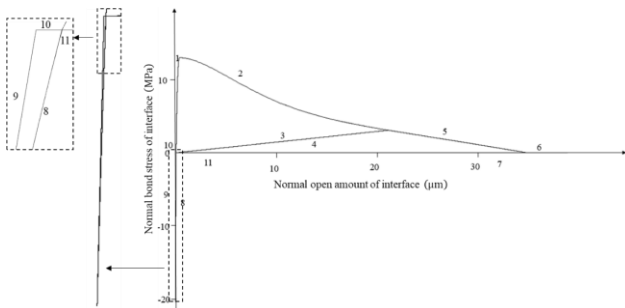


Fig. 5. Compression-tension stress with relative opening-closing displacement in the Mode I test.

3.2. Shearing test

In this simulation, the same model geometry but different boundary conditions were built to validate the shearing behavior of the contact (Fig. 4c). A constant velocity ( $v_x$ ) was exerted at the two side boundaries of the top part of the model. A constant vertical load ( $F_y$ ) was applied to the top boundary of the model to keep contact interfaces in touch. Meanwhile, the contribution of normal stress of contact interface to shear strength (eq. 5), was avoided by setting friction angle to zero. The shear stress and displacement along the interface were tracked during the simulation, and the results are plotted in Fig. 6. The shear stress initially increased with crack slipping until it reached the peak stress (29 MPa) at  $8.34E-07$  (eq. 9). Then the softening stage started, and the shear stress on the fracture surface decreased with slipping until slipping was at  $3.19E-05$  (eq. 10). Under unloading/reloading cycles in this range, contact followed a linear stress displacement path with normal stiffness of  $k_{s,red}$ , which was the ratio of stress to effective displacement at an unloading point. Afterward, the shear stress was equal to the residual shear stress (eq. 7; for  $\sigma_n = 40MPa, |f_{res}| = 3.5MPa$ ). Throughout this procedure, any changes in the direction of applied constant velocity ( $v_x$ ), would directly be seen in the implemented model (e.g., Fig. 2b after breakage of contact interface). It should be noted that unloading/reloading in the pre-peak stage for both tensile and shear simulations was a nonlinear elastic behavior. All the results were in good agreement with the analytical results, suggesting a valid numerical implementation of the CCM.

4. Application of the CCM

This section validates the applicability of the CCM in reproducing the mechanical behavior of rocks under Mixed Mode loading regimes. As the preliminary applications of the CCM, uniaxial and biaxial compression tests were simulated. The contact interface of particles was assigned to the CCM. Damaging and fracturing could only occur along

the interfaces of a block when it exceeded its fracture strength.

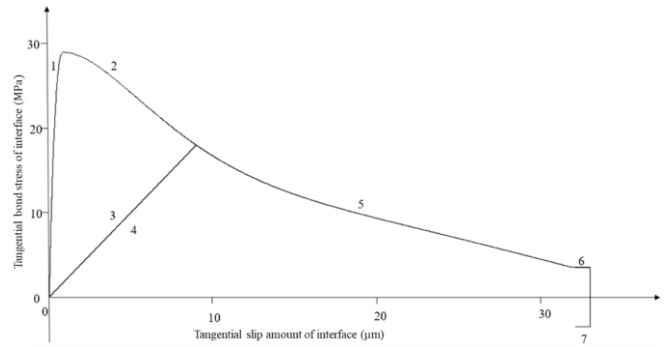


Fig. 6. Shear stress with relative shear displacement in the Mode II test.

In the GBM-DEM approaches, micromechanical parameters are, often, iteratively selected to determine appropriate combinations of micro parameters that approximately reproduce the macroscopic behavior of intact rocks. In this study, micro parameters of the GBM were obtained by a series of laboratory simulation tests, including uniaxial and biaxial compressive strengths. The typical macro properties of carbonate rocks from the Palabora mine were used as calibration targets (listed in Table 1).

Numerical specimens had a width of 50 mm, a height of 125 mm, an average grain edge length of 3 mm, and contained about 755 particles. These specimens were constructed to simulate uniaxial and biaxial compression tests (as shown in Fig. 7). A constant velocity was applied to the upper stiff platen for both uniaxial compressive tests while the lower stiff platen was fixed in both the x and y directions. A preliminary study showed that this velocity rate was sufficiently slow to ensure that the specimen would remain in quasi-static equilibrium throughout the test [1]. The applied axial stress versus the axial strain behavior was measured during the loading process. Compressive stresses were measured in the rectangular domain, as shown in Fig. 7. Nine measurement points were placed at the very top and bottom of the specimen for the compressive test, and the axial strain was recorded during the loading process by dividing the measured axial deformation to the length of the specimen. In addition, the lateral strain was recorded by 24 sets of measuring the horizontal displacement of the measurement points, which were placed at the left and right sides of the specimen.

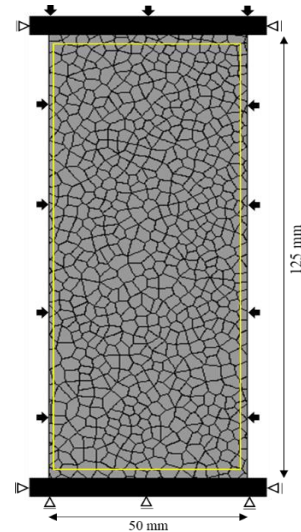
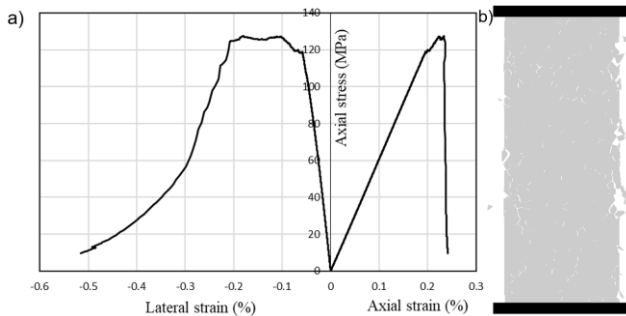


Fig. 7. Layout, boundary conditions, and monitoring the domain of the uniaxial and biaxial compression test.

After conducting a trial and error calibrating procedure, an approximation of the macromechanical behavior was obtained from the numerical tests. The calibrated micromechanical parameters values are listed in Table 1. The sample failed in the brittle mode (Fig. 8). The stress-strain curve of the numerical model under the uniaxial

compression test is shown in Fig. 8b. In general, the macromechanical properties of the carbonate rock samples were adequately approximated, and the numerical model well replicated the failure mode.



**Fig. 8.** Uniaxial compression test a) stress-strain relation, b) final fracture pattern from the numerical simulation.

To derive the macro scale Mohr-Coulomb properties of the rock, i.e., cohesive and friction properties, biaxial compression test simulations were conducted for different confinements of the GBMs-UDEC through linear regression using the equations 13 and 14 [31]. The biaxial compression tests were performed at different confining pressures ranging from 1 to 4 MPa, and the results are shown in Fig. 9. These ranges were chosen to ensure good compliance with the model calibration, which was conducted at low confinement. In the biaxial tests, stresses were applied isotropically to the lateral boundaries (Fig. 7a) and static equilibrium was reached before axial loading. It was observed that as the confining pressure increased, there was a corresponding increase in peak strength. The strength envelopes exhibited approximately a linear relationship for the applied confinement stress range. The obtained cohesion and friction angle for the specimen matched very closely with the typical data reported in Ref. [30] as the simulated cohesion and friction angle were found to be 18.35 MPa and 57.68°, respectively. These results clearly showed that the Voronoi model could properly reproduce the strength of the material under different loading conditions.

$$\varphi = \arcsin \frac{m-1}{m+1} \quad (13)$$

$$c = b \frac{1 - \sin \varphi}{2 \cos \varphi} \quad (14)$$

Where,  $\varphi$  is the friction angle,  $c$  is the cohesion, and  $m$  and  $b$  are the slope and intercept obtained from linear regression of a peak strength versus confining stress plot (Fig. 9).

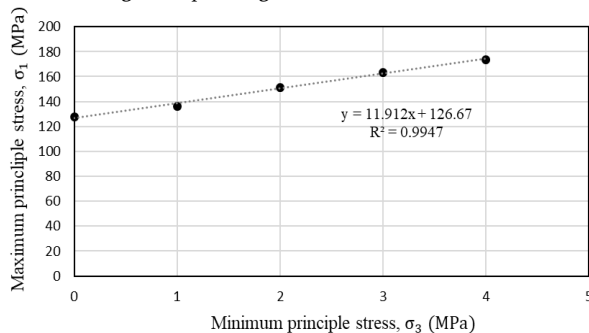


**Fig. 9.** The failure criterion for conventional biaxial compression tests showing the linearity of failure response.

## 5. Conclusions

In this research, the cohesive crack model was successfully implemented under the discrete element code (i.e., UDEC) to account for more realistic simulations of the complex fracturing phenomena of brittle rocks. In order to validate the capability of the implemented CCM when applied to the analyses of brittle rocks, a 2D computational model of Carbonatite rock was tested in numerical uniaxial compression,

tension, and shear tests. The CCM was capable of representing the nonlinear behavior of the contact under different loading regimes. Afterward, in order to determine the validity of the CCM, it was applied in the GBM-UDEC uniaxial and biaxial compression tests. The results showed a perfect match in macroscopic behavior, compared to that of the real rock mass.

## REFERENCES

- [1] Kazerani, T., & Zhao, J. (2010). Micromechanical parameters in bonded particle method for modelling of brittle material failure. *International Journal for Numerical and Analytical Methods in Geomechanics*, 34(18), 1877-1895.
- [2] Fabjan, T., Ivars, D. M., & Vukadin, V. (2015). Numerical simulation of intact rock behaviour via the continuum and Voronoi tessellation models: A sensitivity analysis. *Acta Geotechnica Slovenica*, 12(2), 4-23.
- [3] Park, J. W., Park, C., Song, J. W., Park, E. S., & Song, J. J. (2017). Polygonal grain-based distinct element modeling for mechanical behavior of brittle rock. *International Journal for Numerical and Analytical Methods in Geomechanics*, 41(6), 880-898.
- [4] Lorig, L. J., Watson, A. D., Martin, C. D., & Moore, D. P. (2009). Rockslide run-out prediction from distinct element analysis. *Geomechanics and Geoengineering: An International Journal*, 4(1), 17-25.
- [5] Shin, S. W., Martin, C. D., Park, E. S., & Christiansson, R. (2007). Methodology for estimation of excavation damaged zone around tunnels in hard rock. In *1st Canada-US Rock Mechanics Symposium*.
- [6] Alzo'ubi, A. M. (2009). The effect of tensile strength on the stability of rock slopes. PhD Thesis. Edmonton: University of Alberta; p. 205.
- [7] Lan, H., Martin, C. D., & Hu, B. (2010). Effect of heterogeneity of brittle rock on micromechanical extensile behavior during compression loading. *Journal of Geophysical Research: Solid Earth*, 115(B1).
- [8] Nicksiar, M., & Martin, C. D. (2014). Factors affecting crack initiation in low porosity crystalline rocks. *Rock mechanics and rock engineering*, 47(4), 1165-1181.
- [9] Gao, F., Stead, D., & Elmo, D. (2016). Numerical simulation of microstructure of brittle rock using a grain-breakable distinct element grain-based model. *Computers and Geotechnics*, 78, 203-217.
- [10] Mayer, J. M., & Stead, D. (2017). Exploration into the causes of uncertainty in UDEC grain boundary models. *Computers and Geotechnics*, 82, 110-123.
- [11] Farahmand, K., Vazaios, I., Diederichs, M. S., & Vlachopoulos, N. (2018). Investigating the scale-dependency of the geometrical and mechanical properties of a Moderately jointed rock using a synthetic rock mass (SRM) approach. *Computers and Geotechnics*, 95, 162-179.
- [12] Stavrou, A., & Murphy, W. (2018). Quantifying the effects of scale and heterogeneity on the confined strength of micro-defected rocks. *International Journal of Rock Mechanics and Mining Sciences*, 102, 131-143.
- [13] Itasca (2014). Itasca Consulting Group Inc., The Universal Distinct Element Code (UDEC), Ver. 6.0., Minneapolis, USA.
- [14] Gao, F. Q., & Stead, D. O. U. G. (2014). The application of a modified Voronoi logic to brittle fracture modelling at the laboratory and field scale. *International Journal of Rock*

Mechanics and Mining Sciences, 68, 1-14.

- [15] Nicksiar, M., & Martin, C. D. (2013). Crack initiation stress in low porosity crystalline and sedimentary rocks. *Engineering Geology*, 154, 64-76.
- [16] Potyondy, D. O., & Cundall, P. A. (2004). A bonded-particle model for rock. *International journal of rock mechanics and mining sciences*, 41(8), 1329-1364.
- [17] Cho, N. A., Martin, C. D., & Sego, D. C. (2007). A clumped particle model for rock. *International Journal of Rock Mechanics and Mining Sciences*, 44(7), 997-1010.
- [18] Potyondy, D. O. (2010). A grain-based model for rock: approaching the true microstructure. *Proceedings of rock mechanics in the Nordic Countries*, 9-12.
- [19] Potyondy, D. O. (2012). A flat-jointed bonded-particle material for hard rock. In 46th US Rock mechanics/geomechanics symposium. American Rock Mechanics Association.
- [20] Ding, X., & Zhang, L. (2014). A new contact model to improve the simulated ratio of unconfined compressive strength to tensile strength in bonded particle models. *International Journal of Rock Mechanics and Mining Sciences*, 69, 111-119.
- [21] Kazerani, T., Yang, Z. Y., & Zhao, J. (2012). A discrete element model for predicting shear strength and degradation of rock joint by using compressive and tensile test data. *Rock mechanics and rock engineering*, 45(5), 695-709.
- [22] Elices, M. G. G. V., Guinea, G. V., Gomez, J., & Planas, J. (2002). The cohesive zone model: advantages, limitations and challenges. *Engineering fracture mechanics*, 69(2), 137-163.
- [23] Zang, A., Wagner, F. C., Stanchits, S., Janssen, C., & Dresen, G. (2000). Fracture process zone in granite. *Journal of Geophysical Research: Solid Earth*, 105(B10), 23651-23661.
- [24] Gui, Y., Bui, H. H., & Kodikara, J. (2015). An application of a cohesive fracture model combining compression, tension and shear in soft rocks. *Computers and Geotechnics*, 66, 142-157.
- [25] Dugdale, D. S. (1960). Yielding of steel sheets containing slits. *Journal of the Mechanics and Physics of Solids*, 8(2), 100-104.
- [26] Barenblatt, G. I. (1962). The mathematical theory of equilibrium cracks in brittle fracture. In *Advances in applied mechanics* (Vol. 7, pp. 55-129). Elsevier.
- [27] Hillerborg, A., Mod er, M., & Petersson, P. E. (1976). Analysis of crack formation and crack growth in concrete by means of fracture mechanics and finite elements. *Cement and concrete research*, 6(6), 773-781.
- [28] Evans, R. H., & Marathe, M. S. (1968). Microcracking and stress-strain curves for concrete in tension. *Mat riaux et Construction*, 1(1), 61-64.
- [29] Bandis, S. C., Lumsden, A. C., & Barton, N. R. (1983). Fundamentals of rock joint deformation. In *International Journal of Rock Mechanics and Mining Sciences & Geomechanics Abstracts*, 20(6), pp. 249-268.
- [30] Pine, R. J., Owen, D. R. J., Coggan, J. S., & Rance, J. M. (2007). A new discrete fracture modelling approach for rock masses. *Geotechnique*, 57(9), 757-766.
- [31] Kovari, K., Tisa, A., Einstein, H. H., & Franklin, J. A. (1983). Suggested methods for determining the strength of rock materials in triaxial compression: revised version. *Intl J of Rock Mech & Mining Sci & Geomechanic Abs*, 20(6).